Draft version February 1, 2022
Typeset using LaTeX **twocolumn** style in AASTeX63

arXiv:1912.05215v1 [physics.plasm-ph] 11 Dec 2019

Modeling imbalanced collisionless Alfvén wave turbulence with nonlinear diffusion equations

G. Miloshevich,[1] T. Passot,[1] P.L. Sulem,[1]

[1] *Université Côte d'Azur, CNRS, Observatoire de la Côte d'Azur*
Laboratoire J.L. Lagrange, Boulevard de l'Observatoire, CS 34229, 06304 Nice Cedex 4, France

ABSTRACT

A pair of nonlinear diffusion equations in Fourier space is used to study the dynamics of strong Alfvén-wave turbulence, from MHD to electron scales. Special attention is paid to the regime of imbalance between the energies of counter-propagating waves commonly observed in the solar wind (SW), especially in regions relatively close to the Sun. In the collisionless regime where dispersive effects arise at scales comparable to or larger than those where dissipation becomes effective, the imbalance produced by a given injection rate of generalized cross-helicity (GCH), which is an invariant, is much larger than in the corresponding collisional regime described by the usual (or reduced) magnetohydrodynamics. The combined effect of high imbalance and ion Landau damping induces a steep energy spectrum for the transverse magnetic field at sub-ion scales. This spectrum is consistent with observations in highly Alfvenic regions of the SW, such as trailing edges, but does not take the form of a transition range continued at smaller scales by a shallower spectrum. This suggests that the observed spectra displaying such a transition result from the superposition of contributions originating from various streams with different degrees of imbalance. Furthermore, when imbalanced energy injection is supplemented at small scales in an already fully developed turbulence, for example under the effect of magnetic reconnection, a significant enhancement of the imbalance at all scales is observed.

1. INTRODUCTION

An important contribution to the SW dynamics originates from nonlinear interactions between counter-propagating Alfvén waves. Outgoing waves are emitted at the Sun's surface as a consequence of mechanisms such as reconnection in the chromospheric magnetic network (see e.g. the recent review by Marsch (2018)), which leads to injection of Alfvenic waves at the base of the fast SW (McIntosh 2012). Ingoing waves are created by reflection on density gradients (Chandran & Hollweg 2009; Chandran & Perez 2019) and by velocity shear (Roberts et al. 1992; Breech et al. 2008), or result from parametric decay instability (Vias & Goldstein 1991; Zanna et al. 2001). The energies carried by these counter-propagating waves are usually unequal (Tu et al. 1989; Lucek & Balogh 1998; Wicks et al. 2013), with a degree of "imbalance" depending on the type of wind (Tu et al. 1990; Bruno et al. 2014; Bruno et al. 2017; D'Amicis et al. 2019) and also on the distance from the Sun (Roberts et al. 1987; Marsch & Tu 1990). Accurate in situ observations are now available for the turbulent energy cascades of Alfvén waves (AWs) or, at the sub-ion scales, kinetic Alfvén waves (KAWs) (see e.g. Kiyani et al. (2015); Goldstein et al. (2015) for reviews). A precise understanding of how imbalance affects these cascades is however required in order to predict how much turbulence can heat and accelerate the SW plasma (Chandran et al. 2010; Cranmer et al. 2015; Mallet et al. 2019). Imbalance can also affect cosmic ray scattering efficiency, as for example discussed in Weidl et al. (2015).

While in the MHD range, imbalanced Alfvenic turbulence has been extensively studied both theoretically and numerically (see Chen (2016) for review), its dynamics at sub-ion scales remains largely unexplored. Due to the computational cost of 3D imbalanced kinetic simulations, one is led to develop asymptotic models, isolating the AW dynamics within a spectral range extending from the MHD scales (larger than ion and sonic Larmor radii) to the sub-ion scales, assuming a proton-electron homogeneous plasma subject to a strong ambient magnetic field. Such a description is provided by a Hamiltonian two-field gyrofluid model retaining ion finite Larmor radius (FLR) corrections, parallel magnetic fluctuations and electron inertia (Passot et al. 2018). It takes the form of two dynamical equations for the electron-gyrocenter density and the parallel magnetic potential, from which the electrostatic potential and the parallel magnetic fluctuations are easily derived. Numerical simulations of the two-field gyrofluid are in progress. Here we concentrate on a phenemenological reduction of this model in the form of nonlinear diffusion equations in Fourier space for the transverse spectra of the two conserved quantities, energy and GCH (Passot & Sulem 2019). Concentrating on the effect of imbalance at scales

larger than the electron skin depth d_e, electron inertia is neglected in most of the simulations, which all address the strong turbulence regime.

The model involves drastic simplifications, leaving for future study the influence of effects such as inhomogeneities and wind expansion. In some of the simulations, we nevertheless retain Landau damping which was shown to affect the sub-ion inertial range of balanced AW turbulence (Passot & Sulem 2015; Sulem et al. 2016), but neglect ion cyclotron damping and heating of the medium, considered for example by Cranmer & van Ballegooijen (2003), in spite of their potential effect on the dynamics.

2. THE MODEL

In this section we provide a purely phenomonological derivation of the diffusion model discussed in Passot & Sulem (2019) for the time evolution of the transverse spectra $E(k_\perp,t)$ and $E_C(k_\perp,t)$ of energy and GCH respectively. The latter quantities are related to the energy spectra $E^\pm(k_\perp,t)$ of the counter-propagating waves by $E(k_\perp,t)=E^+(k_\perp,t)+E^-(k_\perp,t)$ and $E_C(k_\perp,t)=(E^+(k_\perp,t)-E^-(k_\perp,t))/v_{ph}(k_\perp)$, where the (parallel) Alfvén phase velocity v_{ph} is a function of $k_\perp$.

A nonlinear diffusion model suitable for three-wave interactions (dominant for KAW turbulence) and preserving the existence of absolute-equilibrium solutions should take the form (Thalabard et al. 2015)

$$\frac{\partial}{\partial t}\frac{E^\pm(k_\perp)}{2}=\frac{\partial}{\partial k_\perp}\Big[D^\mp(E^+,E^-,k_\perp)\frac{\partial}{\partial k_\perp}\frac{E^\pm(k_\perp)}{k_\perp}\Big]+X^\pm, \tag{1}$$

where the corrective terms $X^\pm$ are necessary because the energies of the forward and backward propagating waves are not conserved independently in the presence of dispersion. Due to energy conservation, it is clear that $X^+=-X^-$. The equation for the GCH spectrum then reads

$$\frac{\partial}{\partial t}\frac{E_C}{2} = \frac{2X^+}{v_{\rm ph}}+\Big(\frac{\partial}{\partial k_\perp}+\frac{1}{v_{\rm ph}}\frac{\partial v_{\rm ph}}{\partial k_\perp}\Big)\times \Big\{\sum_{r=\pm1}(-1)^{\frac{r-1}{2}}\frac{D^{(-r)}}{v_{\rm ph}}\frac{\partial}{\partial k_\perp}\Big(\frac{E^{(r)}}{k_\perp}\Big)\Big\}. \tag{2}$$

The invariance of the GCH, which implies that the rhs of (2) should be in a conservative form, allows us to find X^+ by the condition that only the first term in the round parentheses survives. Furthermore, dimensional analysis of the terms involved in Eq. (1), allows us to estimate $D^\mp\sim k_\perp^3/\tau_{\rm tr}^\mp$ in terms of the transfer time $\tau_{\rm tr}^\mp=(\tau_{\rm NL}^\pm)^2/\tau_{\rm w}^\mp$. The case with Landau damping is treated in Appendix A. In its absence, $D^\mp(E^\mp,k_\perp)=C'k_\perp^6\,v_{\rm ph}E^\mp/\widetilde{k}_\parallel^\mp$, where $\widetilde{k}_\parallel^\mp$ measures the inverse parallel correlation length of $\pm$ eddies or wave packets with perpendicular wavenumber $k_\perp$. Here, we used arguments from Passot & Sulem (2019) to fix the nonlinear time $\tau_{\rm NL}^\pm=(k_\perp^3v_{\rm ph}^2E^\pm)^{-1/2}$, consistently with the imbalanced strong MHD turbulence (see Lithwick et al 2007), and also wrote $\tau_{\rm w}^\mp=\widetilde{k}_\parallel^\mp v_{\rm ph}$. The parameter C' can be scaled out in the absence of Landau damping but in its presence affects the location of the transition to the exponential decay (Passot & Sulem 2015). In the following, it is chosen equal to unity. Retaining only strongly local interactions, the model ignores coupling between co-propagating waves since they have nearly the same velocity and can hardly overtake one another and interact. Interactions between such waves with comparable but not quasi-equal wavenumbers were considered by Voitenko & Keyser (2016), but they were shown not to significantly affect the dynamics in the context of the present model (Passot & Sulem 2019).

Assuming that both waves undergo a strong cascade $\tau_{\rm NL}^\pm\sim\tau_{\rm w}^\mp$, we get $\widetilde{k}_\parallel^\pm=(k_\perp^3E^\pm)^{1/2}$. However in MHD it is expected that in the imbalanced case, the + wave (which by definition is more energetic) will undergo a weaker cascade as suggested by Chandran (2008). This effect can be modeled by changing the definition of the parallel wavenumber $\widetilde{k}_\parallel^-$ of the "–" wave subject to interactions with the "+" wave. This suggests to introduce the parameter χ along with the following ansatz

$$\widetilde{k}_\parallel^{(r)}=(k_\perp^3E^{(r)})^{1/2}(E^+/E^-)^{(1-r)\chi/4}. \tag{3}$$

This expression reproduces the different models found in the literature for imbalanced MHD turbulence, depending on the free exponent χ. The value $\chi=0$ corresponds to the model of Lithwick et al. (2007) [1] where both waves are in a strong turbulent regime and satisfy the critical balance condition. In contrast, $\chi=1$ reproduces the model of Chandran (2008), where the transfer time of the stronger wave obeys a weak turbulence phenomenology. The value $\chi=1/4$ corresponds to the model of Beresnyak & Lazarian (2008). Numerical simulations of imbalanced MHD by these authors seem to favor a value of χ larger than zero but also strictly smaller than unity. Differently, in the presence of dispersion, any value of χ smaller than one leads to an unphysical instability at the dissipation scale (Passot & Sulem 2019). The simulations without Landau damping described below (except the purely MHD ones) are thus

[1] In Lithwick et al. (2007), a slightly different interpretation of the critical balance is used where instead of the wave period, the correlation time of the straining imposed by oppositely directed waves is considered. The associated correlation lengths differ from those of our model but the predicted spectra are the same.

performed with $\chi = 1$. The stability range is extended to $\chi \geq 0.5$ when Landau damping is retained.

Finally, the set of reduced equations are cast as

$$\frac{\partial}{\partial t}\frac{E}{2} = \frac{\partial}{\partial k_\perp}\left\{k_\perp^6 V \sum_{r=\pm1} \frac{E^{(-r)}}{\widetilde{k}_\parallel^{(-r)}} \frac{\partial}{\partial k_\perp}\left(\frac{E^{(r)}}{k_\perp}\right)\right\} \tag{4}$$

$$\frac{\partial}{\partial t}\frac{E_C}{2} = \frac{\partial}{\partial k_\perp}\left\{k_\perp^6 \sum_{r=\pm1} \frac{(-1)^{\frac{r-1}{2}} V E^{(-r)}}{v_{ph}\widetilde{k}_\parallel^{(-r)}} \frac{\partial}{\partial k_\perp}\left(\frac{E^{(r)}}{k_\perp}\right)\right\}. \tag{5}$$

In the absence of Landau damping $V = v_{ph}$ (which is the only quantity in the model that incorporates the kinetic effects). It is constant at wavenumbers small compared with the smallest of the inverse ion Larmor radius $\rho_i^{-1} = (\sqrt{2\tau}\rho_s)^{-1}$ (where $\tau = T_{0i}/T_{0e}$ is the ion to electron temperature ratio at equilibrium) and the inverse sonic Larmor radius $\rho_s^{-1} = (\sqrt{m_i/T_{oe}}\Omega_i)^{-1}$ (where m_i is the ion mass and Ω_i the ion gyrofrequency), used as wavenumber unit (with Ω_i^{-1} taken as time unit). It grows linearly ($v_{ph} \approx \alpha k_\perp$) at smaller scales down to $d_e = (2/\beta_e)^{1/2}\delta\rho_s$ (with δ^2 denoting the electron to proton mass ratio), where saturation occurs due to electron inertia.

We treat Landau damping (see Appendix A) by adding dissipative terms $-\gamma E$ and $-\gamma E_C$ in Eqs. (4)-(5) respectively, where $\gamma(k_\perp, \widetilde{k}_\parallel)$ is the AW Landau dissipation rate (dominated by electrons) of transverse and parallel wavenumbers $k_\perp$ and $\widetilde{k}_\parallel = \max(\widetilde{k}_\parallel^+, \widetilde{k}_\parallel^-)$. It also affects (mostly through the ions) the transfer time (Passot & Sulem 2015) and thus modifies the function V entering Eqs. (4)-(5), which becomes $V = v_{ph}^2/(v_{ph} + \mu\sqrt{2\tau})$ where μ is a numerical constant (in the following, $\mu = 3$).

Equations (4)-(5) were solved numerically using a finite difference scheme both in $k_\perp$ (with a logarithmic discretization) and t (using a forward Euler scheme with adaptive time step), modifying a code developed for weak turbulence of gravitational waves (Galtier et al. 2019). We also introduced different grids for the fields and the fluxes, with linear interpolation on the fields. Their coupling ensures better stability.

Simulations were performed for $\beta_e = 2, \tau = 1$ (case I) typical of the SW at 1 AU, and $\beta_e = 0.04, \tau = 10$ (case II), more suitable for regions closer to the Sun (Roytershteyn et al. 2019). For small β_e, d_e significantly exceeds the electron Larmor radius $\rho_e = \sqrt{2}\delta\rho_s$, thus permitting electron inertia to be retained, while electron FLR corrections are neglected. Simulations with and without Landau damping were performed, the latter regime being of interest for comparison with analytical predictions. In this case, hyperdiffusive terms of the form $\nu k_\perp^8 E(k_\perp, t)$ and $\nu k_\perp^8 E_C(k_\perp, t)$, are supplemented

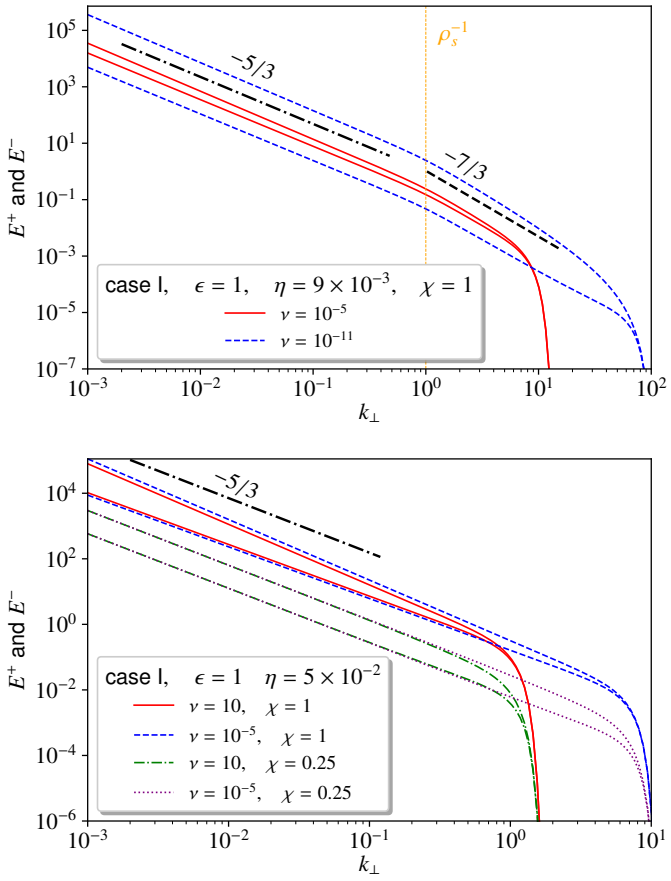


Figure 1. Changes in the imbalance between the $E^\pm$ spectra when, for prescribed energy and GCH transfer rates, the dissipation scale is varied via different values of ν. Top: fully dispersive equations. Bottom: pure MHD regime, where in the $\chi = 0.25$ run, $E^\pm$ are divided by factor 10 for better clarity. Here and in similar further figures, the same color and line style are used for spectra E^+ and E^- corresponding to the same run.

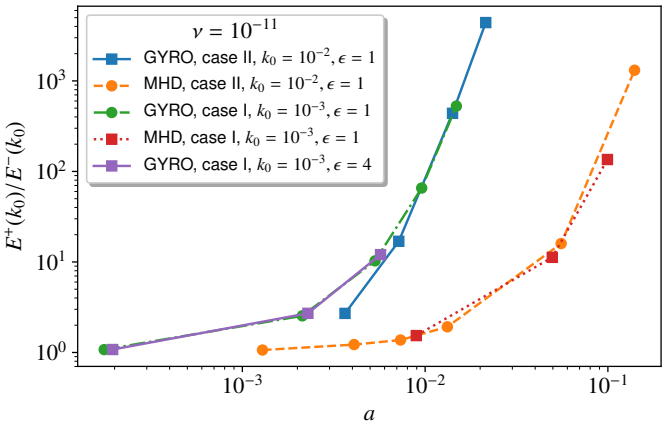


Figure 2. Imbalance at the outer scale k_0 versus $a = \sqrt{2/\beta_e}\eta/\epsilon$ (MHD) and $a = \alpha\eta/\epsilon$ (GYRO), with $\chi = 1$.

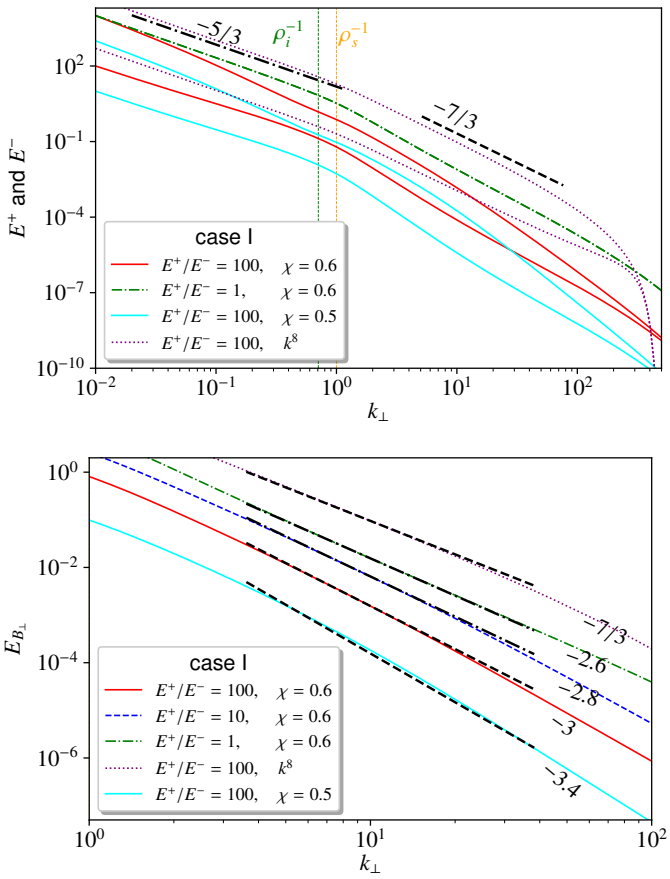


Figure 3. Top: spectra $E^\pm$ when prescribed at the outer wavenumber $k_0 = 10^{-2}$, for four simulations ($\delta = 0$): Landau damping is used in all simulations except when labeled by k^8 . Bottom: Sub-ion $E_{B_\perp}$ spectrum. Curves are shifted vertically for better readability.

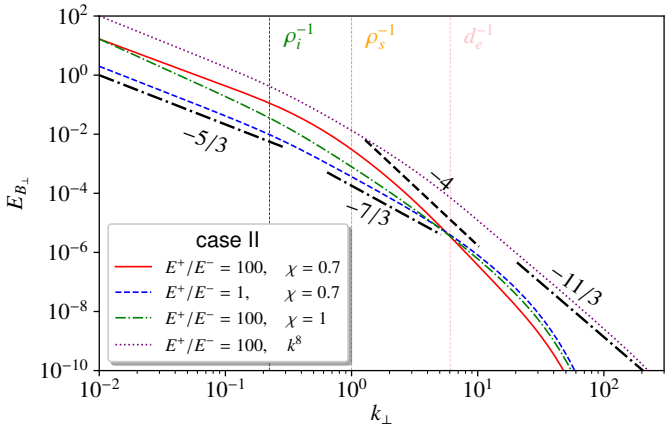


Figure 4. $E_{B_\perp}$ spectrum ($\delta^2 = 1/1836$). As imbalance is increased, spectra get steeper in the presence of Landau damping than with k^8-hyperdiffusion.

in Eqs. (4)-(5), with a coefficient ν depending on the resolution and the parameters. The system is driven at large scale (injection wavenumber k_0), dissipation taking place at small scales (dissipation or pinning wavenumber k_d between 10^1 and 10^4). Driving is performed either through boundary conditions by prescribing the spectra $E^\pm$ or the fluxes η and ϵ of energy and GCH at the smallest wavenumber $k_{\min} = k_0$ (within the range 10^{-3} to 10^{-2}), or differently through injection terms of the form $\varepsilon f(k_\perp)$ and $\eta f(k_\perp)$ supplemented in the r.h.s. of Eqs. (4)-(5), f denoting a function with a compact support located near the injection wavenumber such that $\int_0^\infty f(k_\perp)dk_\perp = 1$. Initial conditions consist of a spectral bump in the MHD range near the smallest retained wavenumber.

3. DIRECT CASCADES IN IMBALANCED TURBULENCE

When, in the absence of Landau damping, Eqs. (4)-(5) are integrated in the strong turbulence regime with prescribed boundary values $E^\pm(k_0)$ and $k_\perp^8$ dissipation terms, we observe a direct transfer of energy and GCH, with the development of power-law spectra which progressively extend to the small scales, up to the moment when the dissipation scale is reached. Although the MHD-range spectrum that forms during this transient is very close to the $k_\perp^{-5/3}$ stationary solution, the sub-ion spectra first develop a balanced regime (as a result of a faster transfer of energy than of GCH) with a spectrum steeper than $k_\perp^{-8/3}$ before converging, while imbalance develops, towards an approximately $-7/3$ steady state when imbalance is weak (not shown). Nonlinear diffusion models for finite-capacity systems (no ultra-violet divergence of the energy) often exhibit such transient anomalous power-law spectra (Thalabard et al. 2015). The case of weak KAW turbulence has recently been addressed by David & Galtier (2019).

When the boundary conditions in k_0 consist of prescribing energy ϵ and GCH η fluxes, the imbalance between E^+ and E^- at large scales is found to strongly depend on the small-scale extension of the dispersive range, as seen in Fig. 1 (top). This is to be compared with Fig. 1 (bottom) where the phase velocity is assumed constant (non-dispersive MHD). Both $\chi = 1$ (for comparison with the dispersive case), and the more realistic value $\chi = 0.25$ are displayed. In both panels, the spectra are plotted at times at which a stationary regime with constant (positive) energy and GCH fluxes have established. In these simulations (case I with $\delta = 0$), we varied the dissipation wavenumber by changing the hyperdiffusivity coefficient. In the MHD regime,

$E^{\pm}$ behave as power laws until the pinning scale is approached. Conversely, in the dispersive case, the spectra approach each other exponentially (consistent with the linear variation of $\phi(k_\perp) = (1/2)\ln(E^+(k_\perp)/E^-(k_\perp))$ when $\alpha\eta/\epsilon \ll 1$ (see Appendix B). It follows that, in contrast with usual hydrodynamic turbulence, large-scale quantities depend on the dissipation scale k_d^{-1}. This effect is much stronger in the presence of dispersion where $E^+(k_0)/E^-(k_0)$ varies exponentially with k_d, while it scales like a power law in MHD when keeping $\chi = 1$ (see Eqs. (B.9) and (B.5) respectively). For MHD with $\chi = 0.25$, the spectra differ by less than 1% from the case $\chi = 0$ for which there is no dependence on k_d (see Eq. (B.12)). To understand heuristically the behavior in the dispersive case, we must note that (i) the dissipative scales for E and E_C are the same since the equation for the GCH spectrum is linear in E_C, (ii) the E_C spectrum steepens at the dispersive scale even more than the energy spectrum since $|E_C(k_\perp)| \leq E(k_\perp)/v_{ph}(k_\perp)$. As a consequence, in order for the GCH dissipation $\nu \int k_\perp^8 E_C dk_\perp$ to match the injected GCH rate η prescribed at k_0, the magnitude of E_C must be larger, and consequently the imbalance at large scales enhanced compared with the MHD problem in the same setting.

Difference between the dispersive (GYRO) and non-dispersive (MHD) cases is also seen on Fig. 2 which displays the imbalance $E^+(k_0)/E^-(k_0)$ at the outer wavenumber $k_0 = k_{\min}$ (located in the MHD range) versus the parameter $a \equiv v_{ph}(k_0)\eta/\epsilon \approx \sqrt{2/\beta_e}\eta/\epsilon$ (MHD) or $a \equiv \alpha\eta/\epsilon$ (GYRO), with α defined in Appendix B, in cases I and II. Graphs corresponding to different β_e collapse on the same curve, with an almost perfect agreement in MHD. Note that, in the GYRO simulations, the assumption $v_{ph} = \alpha k_\perp$ is only approximate, especially close to the ion scale. We furthermore observed that changing ε while keeping η/ε constant has no effect.

Influence of the degree of imbalance in the presence of Landau damping is considered in Fig. 3 in case I with $\delta = 0$, where, for comparison, a simulation involving hyperdiffusion is also presented. Top panel displays the energy spectra $E^{\pm}$, while bottom panel shows the transverse magnetic spectrum $E_{B_\perp}$ (see Appendix C). With hyperdiffusion, the $k_\perp^{-5/3}$ MHD spectrum is continued at sub-ion scales by the classical $k_\perp^{-7/3}$ range, the degree of imbalance significantly decreasing only near the pinning wavenumber. When Landau damping is retained, the degree of imbalance decreases with the scale, the more so when χ is closer to 1 (visible in the top panel when comparing the runs with $E^+(k_0)/E^-(k_0) = 100$ for $\chi = 0.6$ and 0.5). In the sub-ion range, the steepening of $E_{B_\perp}$ displayed in the bottom panel increases with the degree of imbalance (a more pronounced effect when χ is smaller). Such a steepening is often observed as a transition range in the SW at 1AU, depending on the fluctuation power (Bruno et al. 2014), and sometimes associated with proton Landau damping (Sahraoui et al. 2010) and imbalance degree or Alfvenicity (Bruno et al. 2014; Bruno et al. 2017; D'Amicis et al. 2019). The present model suggests that both effects are to act simultaneously. An alternative mechanism for steepening of the spectrum related to reconnection is suggested by Vech et al. (2018).

Figure 4 displays $E_{B_\perp}$ in case II with $\delta^2 = 1/1836$. For this relatively small β_e, an even stronger spectral steepening is observed for large imbalance. Furthermore, the multiplicative factor in the estimate of $E(k_\perp)$ in terms of $E_{B_\perp}(k_\perp)$ is responsible for a steepening of the latter at scales smaller than d_e, an effect visible in particular in the simulation with hyper-diffusivity, $\chi = 1$, and $E^+(k_0)/E^-(k_0) = 100$. A $k_\perp^{-11/3}$ spectrum, classical for balanced IKAW turbulence (Chen & Boldyrev 2017; Passot et al. 2018; Roytershteyn et al. 2019) is still observed for this level of imbalance. Spectra, obtained with Landau damping and electron inertia, are also displayed in this figure: for $\chi = 0.6$ with $E^+(k_0)/E^-(k_0) = 1$ or $E^+(k_0)/E^-(k_0) = 100$, showing that the spectra get steeper as the imbalance increases, and for $\chi = 1$ with $E^+(k_0)/E^-(k_0) = 100$, showing that the steepening is more pronounced as χ is decreased. Such a steepening (although more moderate) is also observed in 3D fully-kinetic simulations (Grošelj et al. 2018).

4. INVERSE TRANSFER OF IMBALANCE

We consider a situation where a stationary turbulence is affected by small-scale injection of KAWs resulting e.g. from magnetic reconnection (Chaston et al. (2005); Liang et al. (2016); Shi et al. (2019) and references therein). We focus on the case where the injection is imbalanced. This setting differs from that used for studying a possible inverse cascade of GCH by driving an initially zero solution. Such a cascade, predicted to exist at sub-ion scales using absolute equilibrium arguments (Passot et al. 2018), and necessarily involving inverse energy transfer, is not captured by the diffusion model and is currently investigated via direct simulations of the gyrofluid model.

In the following, the initial stationary regime is obtained with a large-scale driving at $k_0 = 3.2$ (larger than $k_{\min}$) and a k^8 hyperdiffusivity $\nu = 10^{-16}$ in GYRO and $\nu = 10^{-18}$ in MHD runs. An injection of E^+ energy only (maximal imbalance) is then provided at a wavenumber $k_i = 51.2$ at a rate smaller than or equal to the one imposed at large scales. Stationary solutions are obtained

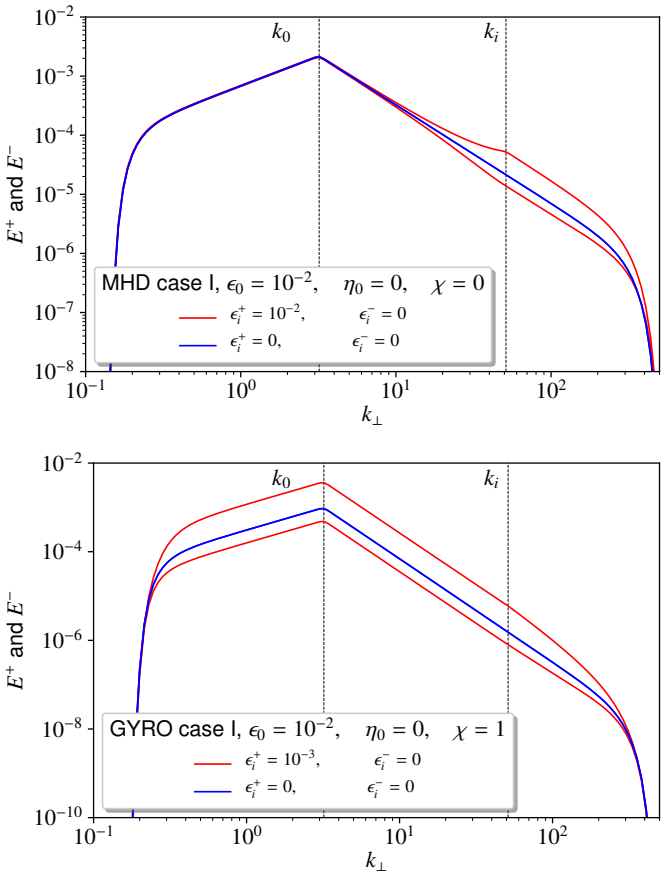


Figure 5. $E^\pm$ spectra in MHD (top) and GYRO (bottom) simulations when GCH is injected at $k_i \gg k_0$ with a rate η_i, in a developed turbulence without Landau damping driven at k_0 with rates ϵ_0 and η_0.

by using a k^{-8} hypodiffusivity equal to 10^{-7} for MHD and 10^{-6} for GYRO. The results presented below pertain to the case where the initial turbulence is balanced but later becomes imbalanced as a result of additional forcing at k_i.

Let us first address the regime where the driving takes place in the MHD range for $\chi = 0$. We see on Fig. 5 (top) that some imbalance is generated at wavenumbers larger than k_i but not at smaller wavenumbers, indicating the absence of inverse transfer of GCH. This point can be understood by solving Eq. (B.11) (right) for $\phi = (1/2)\log(E^+(k_\perp)/E^-(k_\perp))$ with initial condition taken at $k_0 \ll k_\perp < k_i$. For the parameters of the simulation, the initial condition for ϕ is of order unity and the constant C turns out to be very large, leading to a fast decrease of $\phi - \psi$ (where $\psi = 2\tanh^{-1}a$) with $k_\perp$. We thus find that for wavenumbers approaching k_0, the imbalance remains unchanged, equal to the value given by Eq. (B.12). Numerical simulations show that the absence of inverse transfer of GCH still holds for larger values of χ, including in particular 0.25.

When injection takes place in the dispersive range (with $\chi = 1$), assuming that $\alpha\eta/\epsilon \ll 1$, Eq. (B.8) indicates that ϕ is almost independent of $k_\perp$, and thus that the imbalance created at k_i extends to large scales, as exemplified in Fig. 5 (bottom). This evolution results from the development of a transient negative GCH flux at $k_\perp < k_i$ due to the small-scale forcing, leading to a decrease of the total GCH flux and to an enhancement of imbalance that saturates when the flux recovers its original value (consistent with the GCH flux η_0 injected at k_0). In the SW, dispersive scales are always present, making the possibility of such an inverse transfer relevant. It would be of interest to investigate whether the process by which reconnection events can generate an inverse flux towards larger scales (Franci et al. 2017) can also generate imbalance in the case where KAWs are generated at the reconnection sites. The present modeling could also be useful to analyze the recently predicted cascade reversal at d_e in a reduced two-fluid model (Miloshevich et al. 2018) and a 3D extended magnetohydrodynamic model (Miloshevich et al. 2017).

5. CONCLUSION

This letter provides an analysis of the influence of imbalance between the energies of counter-propagating AWs, on the dynamics of a collisionless plasma. It is aimed to contribute to the understanding of regimes encountered in the SW, particularly in regions close to the Sun explored by space missions such as Parker Solar Probe or Solar Orbiter.

The main results can be summarized as follows. (i) The imbalance produced by large-scale injection of GCH at a prescribed rate is enhanced by wave dispersion. (ii) A steep range in the spectrum of the transverse magnetic fluctuations, consistent with the transition region reported in SW observations (Sahraoui et al. 2010), develops at the sub-ion scales, under the combined influence of Landau damping and strong imbalance, an effect enhanced when β_e is decreased. We conjecture that the simulation results can be more specifically related to the observations inside the trailing edge, which is characterized by the highest level of Alfvenicity, i.e. imbalance (Bruno et al. 2014). Existence of a shallower spectrum at smaller scales is then expected to originate from SW regions that are less imbalanced and more energetic at these scales. (iii) Under some conditions the system develops an inverse transfer of imbalance when imbalanced forcing takes place at small scales in an already fully developed turbulence.

Future works include the study of the parent two-field gyrofluid models which is in particular expected to address the question of the characteristic nonlinear time scale in imbalanced turbulence, evaluate the assumption of strongly local interactions and investigate the role of KAW decay instability. The influence on the global dynamics of the coupling of the AWs with the slow modes, important at small β_e as they can generate large-scale parametric decay instabilities, will be studied using an extension of the present gyrofluid including both kinds of waves.

ACKNOWLEDGMENTS

Computations have been done on the "Mesocentre SIGAMM" machine, hosted by Observatoire de la Côte d'Azur.

APPENDIX

A. MODELING LANDAU DAMPING

The dissipation rate $\gamma(k_\perp, k_\parallel)$ is evaluated from Eq. (D.21) of Howes et al. (2006), obtained from the linearized gyrokinetic equations in the limit $\delta^2\tau \ll \beta_i = \tau\beta_e \ll 1$ (c.f. definitions in the text). In a non-dimensional form, one has

$$\gamma = \sqrt{\frac{\pi}{2}}\frac{1}{\beta_e}\Big(\frac{\Gamma_0(\tau k_\perp^2)}{\tau^{3/2}}\exp\Big[-\frac{\overline{\omega}^2}{\tau\beta_e}\Big] + \delta\Big)k_\parallel k_\perp^2. \tag{A1}$$

Here $\overline{\omega}^2 = k_\perp^2(1+\tau-\Gamma_0(\tau k_\perp^2))/(1-\Gamma_0(\tau k_\perp^2))$, where $\Gamma_n(x) = I_n(x)e^{-x}$ and I_n is the first type modified Bessel function of order n. While Eq. (A1) includes both ion and electron Landau damping, at small β_e, the primary contribution comes from electrons, so that Eq. (63) of Howes et al. (2006) can also be used. Landau damping also affects the transfer times $\tau_{tr}^\pm$ of both counter-propagating waves, due to the temperature homogenization process along the magnetic field lines on the correlation length scale $k_\parallel^{\pm-1}$. The associate time scale $v_{th}\widetilde{k}_\parallel^\pm$, which explicitly arises in Landau fluid closures (Snyder et al. 1997; Sulem & Passot 2015), being proportional to the thermal velocity v_{th} of the particles, is very short for the electrons and cannot affect the dynamics. It is in contrast relevant in the case of the ions for which it is given in the present units by $(\tau_H^\pm)^{-1} = \mu\sqrt{2\tau}\,\widetilde{k}_\parallel^\pm$, where μ denotes a numerical constant of order unity. We are thus led to write

$$\tau_{tr}^\pm = \tau_{NL}^\pm\left(\frac{\tau_{NL}^\pm}{\tau_w^\pm} + \frac{\tau_{NL}^\pm}{\tau_H^\pm}\right), \tag{A2}$$

which leads to

$$V = \frac{v_{ph}^2}{v_{ph} + \mu\sqrt{2\tau}}. \tag{A3}$$

B. IMBALANCED REGIME

It is possible to relate the flux ratio η/ϵ to the imbalance $E^+(k_0)/E^-(k_0)$ at the outer scale. This can be done by rewriting the spectra in the form

$$\frac{E(k_\perp)}{k_\perp} = \rho(k_\perp)\cosh\phi(k_\perp), \qquad \frac{v_{ph}(k_\perp)E_C(k_\perp)}{k_\perp} = \rho(k_\perp)\sinh\phi(k_\perp). \tag{B.1}$$

This leads to

$$E^\pm(k_\perp) = \frac{1}{2}k_\perp\rho(k_\perp)e^{\pm\phi(k_\perp)}. \tag{B.2}$$

Two cases are to be distinguished, depending on the value of χ.

B.1. *The case* $\chi = 1$

From Eq. (4) we see that, in the case $\chi = 1$, solutions with constant fluxes η and ϵ obey

$$\frac{d}{dk_\perp}\rho^2(k_\perp) = -\frac{2\varepsilon\,\widetilde{k}_\parallel^+(k_\perp)}{k_\perp^7 v_{ph}(k_\perp)}, \qquad \rho^2(k_\perp)\frac{d}{dk_\perp}\phi(k_\perp) = -\frac{\eta\,\widetilde{k}_\parallel^+(k_\perp)}{k_\perp^7}, \tag{B.3}$$

where $\widetilde{k}_\parallel^+ = k_\perp^2\sqrt{\rho/2}\exp(\phi/2)$.

- In the MHD regime where $v_{ph} = \sqrt{2/\beta_e}$, it is easily shown that, defining $a = \eta v_{ph}/\epsilon$,

$$\phi = \phi_0 + a \ln \rho/\rho_0. \tag{B.4}$$

When substituted into Eq. (B.3, left), this leads to $\rho = \left((3-a)\, e^{\phi_0/2}\epsilon\sqrt{\beta_e}/16\right)^{2/3} k_0^{-8/3}(k_\perp/k_0)^{-8/(3-a)}$, which, after some algebra, prescribes for the MHD regime

$$\frac{E^+(k_0)}{E^-(k_0)} = \left(\frac{k_d}{k_0}\right)^{\frac{16a}{3-a}}, \quad \phi = \phi_0 - \frac{8a}{3-a}\ln\frac{k_\perp}{k_0}, \tag{B.5}$$

where k_d denotes the pinning wavenumber. This prediction excellently matches the numerical results presented in Fig. 2.

- In the far sub-ion range, $v_{ph} \approx \alpha k_\perp$, where $\alpha = 2\sqrt{\dfrac{1+\tau}{\beta_e(2+(1+\tau)\beta_e)}}$. The relationship between ρ and ϕ derived from Eq. (B.3) reads in this case

$$\frac{\alpha\eta}{\epsilon} k_\perp \frac{d}{dk_\perp}\ln\rho = \frac{d\phi}{dk_\perp}. \tag{B.6}$$

If we assume $\eta\alpha/\epsilon \ll 1$, ϕ can be approximated by a constant ϕ_0 in Eq. (B.3, left) which is then solved as

$$\rho = \left(\frac{3\,\epsilon\, e^{\phi_0/2}\sqrt{\beta}}{10\alpha\sqrt{2}}\right)^{2/3} k_\perp^{-10/3}. \tag{B.7}$$

Equation (B.6) becomes

$$\phi = \phi_0' - \frac{10}{3}\frac{\alpha\eta}{\epsilon}k_\perp, \tag{B.8}$$

which determines the pinning wavenumber k_d where ϕ vanishes. From Eq. (B.2), it is clear that for small $\alpha\eta/\epsilon$, ϕ will be nearly constant up to the vicinity of k_d where the spectra $E^\pm$ approach each other exponentially. Therefore, we can obtain a dispersive imbalance relation, whose behavior is very different from the MHD case, namely

$$\frac{E^+(k_0)}{E^-(k_0)} = \exp\left(\frac{20\alpha\eta(k_d-k_0)}{3\epsilon}\right), \quad \phi_0' = \frac{10\alpha\eta k_d}{3\epsilon} \quad \text{when} \quad k_d \gg k_0. \tag{B.9}$$

To apply this formula to the case where both MHD and dispersive ranges are present, one has to match ϕ at the transition wavenumber $k_\perp$ using both (B.5) and (B.8). But the contribution due to the second term in (B.5) is negligible and therefore we can simply extend (B.9) to the full range.

B.2. *The MHD regime with $\chi = 0$*

After some algebra, it is easy shown that the equations for ρ and ϕ read

$$\rho\frac{d}{dk_\perp}\left(\rho^{1/2}(k_\perp)\cosh(\frac{\phi(k_\perp)}{2})\right) = -\frac{\epsilon}{2^{3/2}k_\perp^5 v_{ph}}, \qquad \rho\frac{d}{dk_\perp}\left(\rho^{1/2}(k_\perp)\sinh(\frac{\phi(k_\perp)}{2})\right) = -\frac{\eta}{2^{3/2}k_\perp^5}. \tag{B.10}$$

From here, defining $\tanh\psi/2 = \eta v_{ph}/\epsilon$, we derive ($A$ being a constant),

$$\sqrt{\rho}\sinh\frac{\phi-\psi}{2} = A, \quad \frac{d\phi}{dk} = \frac{C}{k_\perp^5}\sinh^4\frac{\phi-\psi}{2}, \tag{B.11}$$

where $C = \dfrac{\epsilon/v_{ph}}{2^{1/2}\,A^3\cosh\psi/2}$. Let us consider the case where energy and GCH are injected at $k_\perp = k_i$. Imposing $\rho = 0$ as boundary condition at $k_\perp = +\infty$, we find that $A = 0$. As a result $\phi = \psi$ for $k_\perp > k_i$. In this case, the imbalance becomes independent of $k_\perp$ in the form

$$\frac{E^+(k_\perp)}{E^-(k_\perp)} = \left(\frac{\epsilon+\eta v_{ph}}{\epsilon-\eta v_{ph}}\right)^2. \tag{B.12}$$

We also get $\rho^{3/2} = \dfrac{3\epsilon\sqrt{\beta_e}}{16\,k_\perp^4}\cosh^{-1}\frac{\psi}{2}$. For $k_\perp < k_i$, where we can assume $\psi = 0$ (in the absence of GCH injection at k_0), we can deduce from Eq. (B.11, right) (using that the constant C is large as a result of the small value of ρ at k_i) that ϕ also tends to zero, as it is observed in the simulations of the diffusion model (Fig. 5, bottom). This explains the absence of propagation of the imbalance to large scales.

C. TRANSVERSE MAGNETIC ENERGY SPECTRUM

The transverse magnetic energy spectrum $E_{B_\perp}$, commonly measured in the SW, can be related, at least approximately, to the total energy spectrum. Writing $\boldsymbol{k} = (k_\perp, \theta, k_\parallel)$ in cylindrical coordinates, the total energy can be expressed as $\mathcal{E} = \int E(k_\perp)dk_\perp$, with an energy spectrum given by $E(k_\perp) = (1/2)\int(s^2|k_\perp L_e\widehat{A}_\parallel|^2 + |k_\perp L_e\Lambda\widehat{\varphi}|^2)dk_\parallel k_\perp d\theta$, equivalent to Eq. (2.36) of Passot & Sulem (2019). Here, $\widehat{\varphi}(\boldsymbol{k})$ and $\widehat{A}_\parallel(\boldsymbol{k})$ refer to the Fourier transforms of the electrostatic and parallel magnetic potentials respectively, $L_e = (1 + 2\delta^2 k_\perp^2/\beta_e)^{1/2}$ and Λ defined in Eq. (2.17) of Passot & Sulem (2019)) is a function of $k_\perp$ which tends to 1 as $k_\perp \to 0$ and is proportional to $1/k_\perp$ in the sub-ion range. The first term in the integral rewrites $L_e^2 E_{B_\perp}$, where $E_{B_\perp} = (s^2/2)\int|\widehat{B}_\perp(\boldsymbol{k})|^2 dk_\parallel k_\perp d\theta$ corresponds to the magnetic energy spectrum, and the second one reduces in the MHD regime to the kinetic energy spectrum. Their difference, referred to as the residual energy spectrum, is observed to remain small if initially zero in direct numerical simulations of the parent gyrofluid. In spite of the nonlinear interactions, the solution can indeed be viewed as a superposition of eigenmodes of both polarizations (which satisfy $s^2|k_\perp L_e\widehat{A}_\parallel|^2 = |k_\perp L_e\Lambda\widehat{\varphi}|^2$), and we are thus led to write $E_{B_\perp}(k_\perp) \approx (1/2)L_e^{-2}E(k_\perp)$.

REFERENCES

Beresnyak, A., & Lazarian, A. 2008, Astrophys. J, 682, 1070

Breech, B., Matthaeus, W. H., Minnie, J., et al. 2008, J. Geophys. Res.: Space Phys., 113, A08105

Bruno, R., Telloni, D., DeIure, D., & Pietropaolo, E. 2017, Month. Not. R. Astro. Soc., 472, 1052

Bruno, R., Trenchi, L., & Telloni, D. 2014, Astrophys. J. Lett., 793, L15

Chandran, B. D. G. 2008, Astrophys. J., 685, 646

Chandran, B. D. G., & Hollweg, J. V. 2009, Astrophys. J., 707, 1659

Chandran, B. D. G., Li, B., Rogers, B. N., Quataert, E., & Germaschewski, K. 2010, Astrophys. J., 720, 503

Chandran, B. D. G., & Perez, J. C. 2019, J. Plasma Phys., 85, 905850409

Chaston, C. C., Phan, T. D., Bonnell, J. W., et al. 2005, Phys. Rev. Lett., 95, 065002

Chen, C. H. K. 2016, J. Plasma Phys., 82, 535820602

Chen, C. H. K., & Boldyrev, S. 2017, Astrophys. J., 842, 122

Cranmer, S. R., Asgari-Targhi, M., Miralles, M. P., et al. 2015, Phil. Trans. R. Soc. London, A373, 20140148

Cranmer, S. R., & van Ballegooijen, A. A. 2003, Astrophys. J., 594, 573

D'Amicis, R., Matteini, L., & Bruno, R. 2019, Month. Not. R. Astro. Soc., 483, 4665

David, V., & Galtier, S. 2019, Astrophys. J. Lett., 880, L10

Franci, L., Cerri, S. S., Califano, F., et al. 2017, Astrophys. J. Lett., 850, L16

Galtier, S., Nazarenko, S. V., Buchlin, E., & Thalabard, S. 2019, Physica D, 390, 84

Goldstein, M. L., Wicks, R. T., Perri, S., & Sahraoui, F. 2015, Phil. Trans. R. Soc. A, 373, 20140147

Grošelj, D., Mallet, A., Loureiro, N. F., & Jenko, F. 2018, Phys. Rev. Lett., 120, 105101

Howes, G. G., Cowley, S. C., Dorland, W., et al. 2006, Astrophys. J., 651, 590

Kiyani, K. H., Osman, K. T., & Chapman, S. C. 2015, Phil. Trans. R. Soc. A, 373, 20140155

Liang, J., Lin, Y., Johnson, J. R., Wang, X., & Wang, Z.-X. 2016, J. Geophys. Res.: Space Phys., 121, 6526

Lithwick, Y., Goldreich, P., & Sridhar, S. 2007, Astrophys. J., 655, 269

Lucek, E. A., & Balogh, A. 1998, Astrophys. J., 507, 984

Mallet, A., Klein, K. G., Chandran, B. D. G., et al. 2019, J. Plasma Phys., 85, 175850302

Marsch, E. 2018, Ann. Geophys., 36, 1607

Marsch, E., & Tu, C.-Y. 1990, J. Geophys. Res., 95 (A6), 8211

McIntosh, S. W. 2012, Space Sci. Rev., 172, 69

Miloshevich, G., Lingam, M., & Morrison, P. J. 2017, New J. Phys., 19, 015007

Miloshevich, G., Morrison, P. J., & Tassi, E. 2018, Phys. Plasmas, 25, 072303

Passot, T., & Sulem, P. L. 2015, Astrophys. J. Lett., 812, L37

—. 2019, J. Plasma Phys, 85, 905850301

Passot, T., Sulem, P. L., & Tassi, E. 2018, Phys. Plasmas, 25, 042107

Roberts, D. A., Goldstein, M. L., Klein, L. W., & Matthaeus, W. H. 1987, J. Geophys. Res.: Space Phys., 92, 12023

Roberts, D. A., Goldstein, M. L., Matthaeus, W. H., & Ghosh, S. 1992, J. Geophys. Res.: Space Phys., 97, 17115

Roytershteyn, V., Boldyrev, S., Delzanno, G. L., et al. 2019, Astrphys. J., 870, 103

Sahraoui, F., Goldstein, M. L., Belmont, G., Canu, P., & Rezeau, L. 2010, Phys. Rev. Lett., 105

Shi, P., Huang, K., Lu, Q., & Sun, X. 2019, Plasma Phys. Control. Fusion, 61, 125010

Snyder, P. B., Hammett, G. W., & Dorland, W. 1997, Phys. Plasmas, 4, 3974

Sulem, P. L., & Passot, T. 2015, J. Plasma Phys., 81, 325810103

Sulem, P. L., Passot, T., Laveder, D., & Borgogno, D. 2016, Astrophys. J., 818, 66

Thalabard, S., Nazarenko, S., Galtier, S., & Medvedev, S. 2015, J. Phys. A: Math. Theor., 48, 285501

Tu, C. Y., March, E., & Rausenbauer, H. 1990, Geophys. Res. Lett., 17, 283

Tu, C.-Y., Marsch, E., & Thieme, K. M. 1989, J. Geophys. Res., 94 (A9), 11739

Vech, D., Mallet, A., Klein, K. G., & Kasper, J. C. 2018, Astrophys J., L27

Vias, A. F., & Goldstein, M. L. 1991, J. Plasma Phys., 46, 129152

Voitenko, Y., & Keyser, J. D. 2016, Astrophys. J. Lett., 832, L20

Weidl, M. S., Jenko, F., Teaca, B., & Schlickeiser, R. 2015, Astrophys. J., 811, 8

Wicks, R. T., Roberts, D. A., Mallet, A., et al. 2013, Astrophys. J., 778, 177

Zanna, L. D., Velli, M., & Londrillo, P. 2001, Astron. & Astrophys., 367, 705